

# Tilting-Sensitive Triboelectric Nanogenerators for Energy Harvesting from Unstable/Fluctuating Surfaces

Wei Zhong, Liang Xu, Haiming Wang, Jie An, and Zhong Lin Wang\*

The invention of triboelectric nanogenerators provides an opportunity to utilize previously wasted mechanical energy. The sway energy of ships that affects navigation and comfort on board has been considered negative in the past. Here, a tilting-sensitive triboelectric nanogenerator (TS-TENG) that can effectively harvest energy from unstable/fluctuating surfaces is demonstrated by using the sway energy of ships. The device adopts integrated blade structures on sliders, which make it sensitive to tilts and guarantee its power output. The response of the device to tilt agitations of different slopes and frequencies is systematically investigated. Rotational symmetry configuration is used to improve the motion stability of the device by excluding extra torque on the sliders. The peak power density and average power density of the TS-TENG can reach 1.41 and 0.1 W m<sup>-3</sup>, respectively, in low-frequency and low-amplitude fluctuating conditions. By the excellent performance of harvesting energy from unstable/fluctuating surfaces, the TS-TENG is considered promising for powering various distributed sensor devices on the ship for smart ships.

## 1. Introduction

There exist various forms of energy in nature that human has utilized for sustainable development, such as light energy, chemical energy, mechanical energy, and nuclear energy.<sup>[1]</sup> Among them mechanical energy is widely distributed in different scales. Nowadays, the power generation from mechanical energy mainly relies on electromagnetic generators (EMGs), which are costly, cumbersome and inefficient under conditions of low frequencies and low amplitudes.<sup>[2]</sup> Thus a

new generator is required to work complementarily or even replace the EMG in some situations. The invention of triboelectric nanogenerators (TENGs) in 2012 provides a new principle to convert mechanical energy into electricity.<sup>[2b,3]</sup> The TENG works based on triboelectrification and electrostatic induction.<sup>[4]</sup> It has the merits of low cost, easy fabrication, abundant material choices and device forms.<sup>[2b]</sup> Most importantly, the TENG can harvest mechanical energy of low frequencies and low amplitudes more efficiently, providing an opportunity to turn widespread wasted mechanical energy into electricity.<sup>[2a,c]</sup> Since its invention, it has been demonstrated to harvest various types of mechanical energy successfully from the environment or from the body of humans, such as water wave,<sup>[5]</sup> wind,<sup>[6]</sup> vibration,<sup>[7]</sup> walking,<sup>[8]</sup> etc. The harvested energy can be applied to drive small electronics to ful-

fill the power requirement of such widely distributed devices that need effective energy supply.<sup>[2b,4b,9]</sup> The sway of ships, which contains considerable energy, is regarded as negative effect in the past, because it can bring danger to navigation and affect comfort on board. Considering the sway of ships is usually in the form of low-frequency and low-amplitude fluctuation, TENG should be effective to harvest such kind of energy for various applications, such as smart ships with widespread sensing nodes, converting the energy into useful forms.

In this work, a tilting-sensitive triboelectric nanogenerator (TS-TENG) that can harvest energy from unstable/fluctuating surfaces is demonstrated, making use of the sway energy of ships. The device uses integrated blade structures on sliders, enabling its sensitivity to low-frequency and low-amplitude agitations. The response of the device to different tilt agitations is systematically investigated. Model ship experiments in wave tanks provide its output characteristics in water, showing good performance in harvesting sway energy.

## 2. Results and Discussion

The structure of the TS-TENG is schematically shown in Figure 1a,b. There are two major parts in this device, namely, Frame 1 with 14 PTFE (polytetrafluoroethylene) blades fixed on the frame and Frame 2 with 15 Al (aluminum) blades fixed. The two parts intersect each other and form 28 fundamental TENG units, as shown in Figure 1b. Sliders are mounted to connect

W. Zhong, Dr. L. Xu, H. Wang, J. An, Prof. Z. L. Wang  
CAS Center for Excellence in Nanoscience  
Beijing Key Laboratory of Micro-Nano Energy and Sensor  
Beijing Institute of Nanoenergy and Nanosystems  
Chinese Academy of Sciences  
Beijing 100083, China  
E-mail: zhong.wang@mse.gatech.edu

W. Zhong, Dr. L. Xu, H. Wang, J. An, Prof. Z. L. Wang  
School of Nanoscience and Technology  
University of Chinese Academy of Sciences  
Beijing 100049, China  
Prof. Z. L. Wang  
School of Material Science and Engineering  
Georgia Institute of Technology  
Atlanta, GA 30332, USA

 The ORCID identification number(s) for the author(s) of this article can be found under <https://doi.org/10.1002/adfm.201905319>.

DOI: 10.1002/adfm.201905319

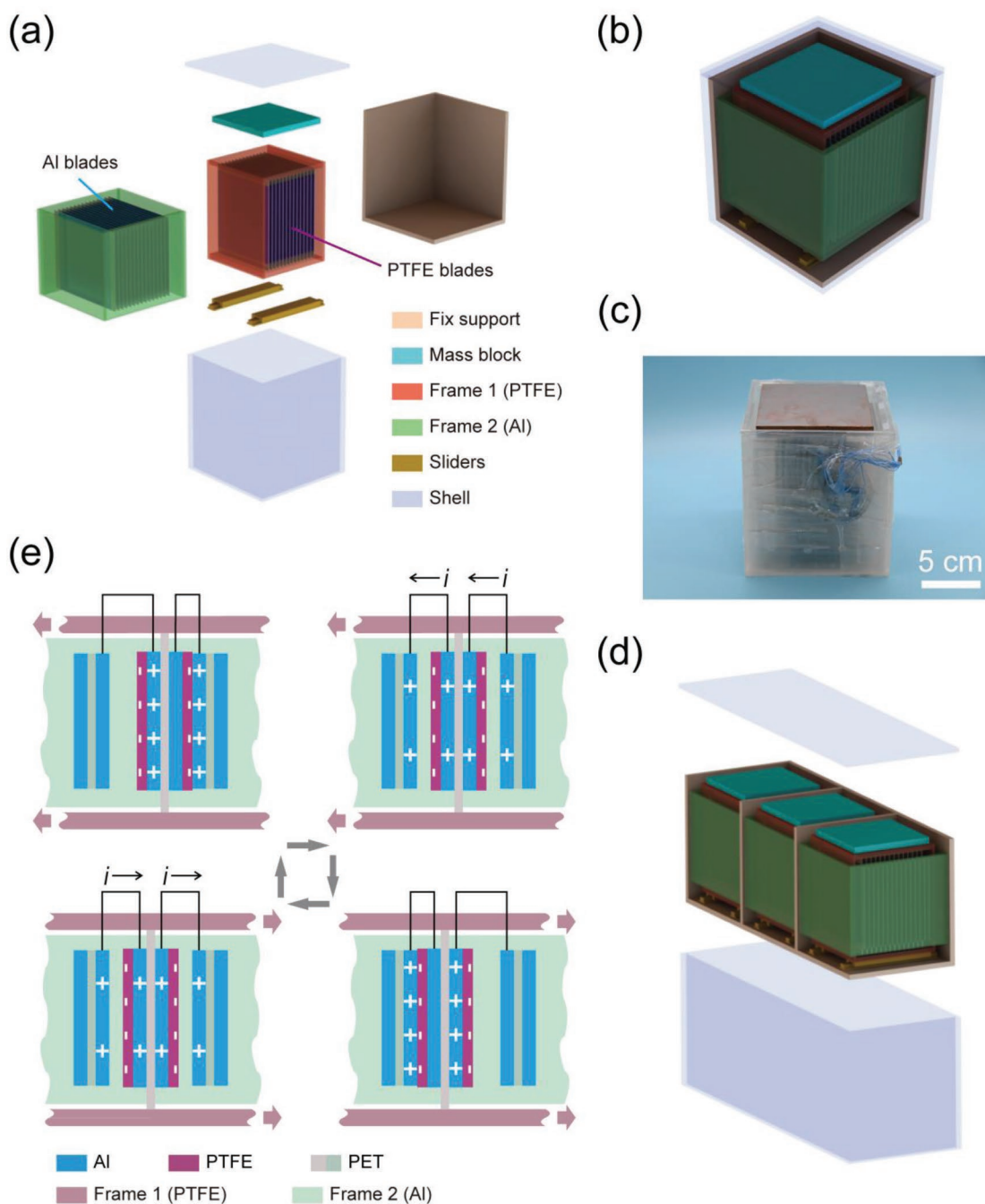


**Figure 1.** Structure and working principle of the TS-TENG device. Schematic explosive view a) and schematic view b) of the device. c) Photograph of the TS-TENG. d) Integrated array of multiple devices. e) Operation principle of the device.

the bottom of Frame 1 and the fix support, enabling sliding of Frame 1 on the fix support. A mass block is fixed on the top of Frame 1 to enhance the inertial force and gravity. Frame 2 is fixed on the side wall of the fix support as a stationary part. The fix support is then placed in the packaging shell to protect the TS-TENG from water intrusion and maintain constant internal humidity during operation. The design ensures that Frame 1 can respond well to the tilts of fluctuating surfaces and slide reciprocally in the shell to produce contact and separation

motion between the PTFE blades and the Al blades. A fabricated device is shown in Figure 1c. Figure 1d demonstrates that the structure can be duplicated into large scale arrays which will enhance the total output.

The detailed structure of the TENG units and the basic working mechanism is shown in Figure 1e. The TS-TENG is based on the vertical contact-separation mode for harvesting mechanical energy. The two types of blades, namely, the PTFE blades and the Al blades, appear alternatively, and each two

adjacent blades can form a fundamental TENG unit. The structure of the PTFE blade is two PTFE films with back Al electrodes attached to a poly(ethylene terephthalate) (PET) substrate sheet, and the Al blade is constituted by attaching two Al friction electrodes to a PET sheet. The operation mechanism of fundamental TENG units is based on tribo-electrification and electrostatic induction.<sup>[4a,10]</sup> As shown in Figure 1e, when the PTFE film is in contact with the Al friction electrode, due to the difference in charge affinity, the surface of the PTFE film will gain negative static charges and the Al friction electrode will be positively charged.<sup>[11]</sup> With the sliding of Frame 1, separation of the PTFE film and the Al friction electrode will take place. The accompanied separation of charges with different signs will cause a potential difference between the Al friction electrode and the Al back electrode. Electrons will transfer from the Al back electrode to the Al friction electrode to compensate the potential difference, forming current in the external circuit. A reverse current will be generated when the PTFE film and the Al friction electrode get into contact again accompanying the sliding back of Frame 1. Thus, the TS-TENG can produce alternate current output with reciprocal sliding of Frame 1 agitated by surface tilts. Owing to that each blade has two sides, when one side is going to contact, the other side is inevitable in a state of gradual separation. The TENG units of the device will output in two different phases, which requires rectification to produce parallel connected output.

In order to characterize the basic output performance of the TS-TENG, experiments simulating surface fluctuation by a linear motor were conducted in air. Schematic illustration of the experimental setup is shown in Figure 2a. A base plate pulled by the linear motor through a rope to produce an angular displacement was used to simulate the unstable surface. The TS-TENG was fixed on the base plate in the experiments. First, the base plate is parallel to the horizontal plane, and the TS-TENG is also in a horizontal state, where neither of the two sides (noted as the A side and the B side) is in contact (State I). When the rope is released by the linear motor, the base plate and the device will roll counterclockwise to form an angle  $-\alpha$  with the horizontal plane, and Frame 1 inside the device will slide down to the left in response to the slope due to gravity (State II). The A side of blades is in contact and the B side of blades is in separation, outputting a current  $i_A$  from the back electrode of the PTFE film to the Al friction electrode in the A side and another current  $i_B$  from the Al friction electrode to the back electrode of the PTFE film in the B side, respectively. When the rope is pulled up by the linear motor, a tilt to the right is formed and the base plate with clockwise roll will form an angle  $+\alpha$  with the horizontal plane. Due to the inclination, Frame 1 inside the device will slide down to the right (State III). In this state, the A side is in separation and the B side is in contact respectively, causing  $i_A$  flowing from the friction electrode to the back electrode of the PTFE film and  $i_B$  flowing from the back electrode of the PTFE film to the friction electrode. Periodical repeating of the states will produce continuous output of such currents. To merge the two alternate currents in different phases for a total output of the TS-TENG, a circuit using two rectification bridges was adopted, as shown in Figure 2b. Due to the simple two states of the TENG that are easy to be synchronized among different devices in the sway

of ships, even for large scale TENG arrays shown in Figure 1d, only two rectifiers are needed which will greatly simplify the output circuit.

The output of both sides of the TS-TENG agitated by the linear motor in air is shown in Figure 2c–e. The transferred charges of the A side and the B side are 0.92 and 1.13  $\mu\text{C}$ , respectively. The peak short-circuit currents of the A side and the B side are 23.82 and 24.66  $\mu\text{A}$ , respectively. The peak-to-peak output voltages of the A side and the B side are 127.64 and 124.31 V, respectively. Further investigation of the rectified current with different slopes and frequencies is shown in Figure 2f,g. When the frequency was fixed at 1.2 Hz, the rectified current improved with larger slopes, reaching 51.26  $\mu\text{A}$  at the slope of 15.9°. And the device can have output even in very small slopes as 2.2°, demonstrating the sensitivity of the device to tiny slopes. When the slope was fixed at 9°, the rectified current improved with the rising of the frequency, reaching 28.24  $\mu\text{A}$  at the frequency of 1.4 Hz (Figure 2g). The rectified current at 1.2 Hz and 9° in Figure 2f,g is about 27  $\mu\text{A}$ . The output power is an important indication of the electricity-generation capability of the device. The peak power  $P_{\text{peak}}$  and average power  $P_{\text{ave}}$  of the device with different resistive loads are shown in Figure 2h. At the frequency of 1.2 Hz and the slope of 9°, a highest peak power of 3.63 mW and a highest average power of 0.32 mW were obtained respectively, and the best matching resistance is about 20.6 M $\Omega$ . The power is calculated according to the following equations

$$P_{\text{peak}} = I_{\text{peak}}^2 R \quad (1)$$

$$P_{\text{ave}} = \frac{\int_0^T I^2 R dt}{T} \quad (2)$$

where  $R$  is the load resistance,  $T$  is the period of the output,  $I$  is the output current, and  $I_{\text{peak}}$  is the peak value of the current. The highest peak power density is 1.8  $\text{W m}^{-3}$  and the highest average power density is 0.16  $\text{W m}^{-3}$ , indicating that the device has good energy harvesting ability from unstable/fluctuating surfaces.

In order to use the device to drive high-power electronic devices, a capacitor as an energy storage component is needed. The charging curves of different capacitors are shown in Figure 2i. A capacitor of 100  $\mu\text{F}$  can be charged to 5.25 V for only 120 s, and the amount of stored charges is 525  $\mu\text{C}$  with the agitation frequency of 1.2 Hz and the slope of 9°.

As a sensitive fluctuating-surface energy harvester, the performance of the TS-TENG for harvesting ship sway energy in water was then investigated. The statuses of the device with ship tilts are schematically shown in Figure 3a. External forces, such as wind and wave, can cause the ship to depart from the equilibrium and tilts. Meanwhile, the interplay of the gravity force and the buoyant force of the ship after the ship leave its equilibrium position can cause continuous sway. The induced slopes will make Frame 1 in the TS-TENG slide to the left or right. More specifically, when the ship is in an equilibrium position, the gravity of the ship and water buoyancy are equal with opposite directions (State I). The shipborne TS-TENG

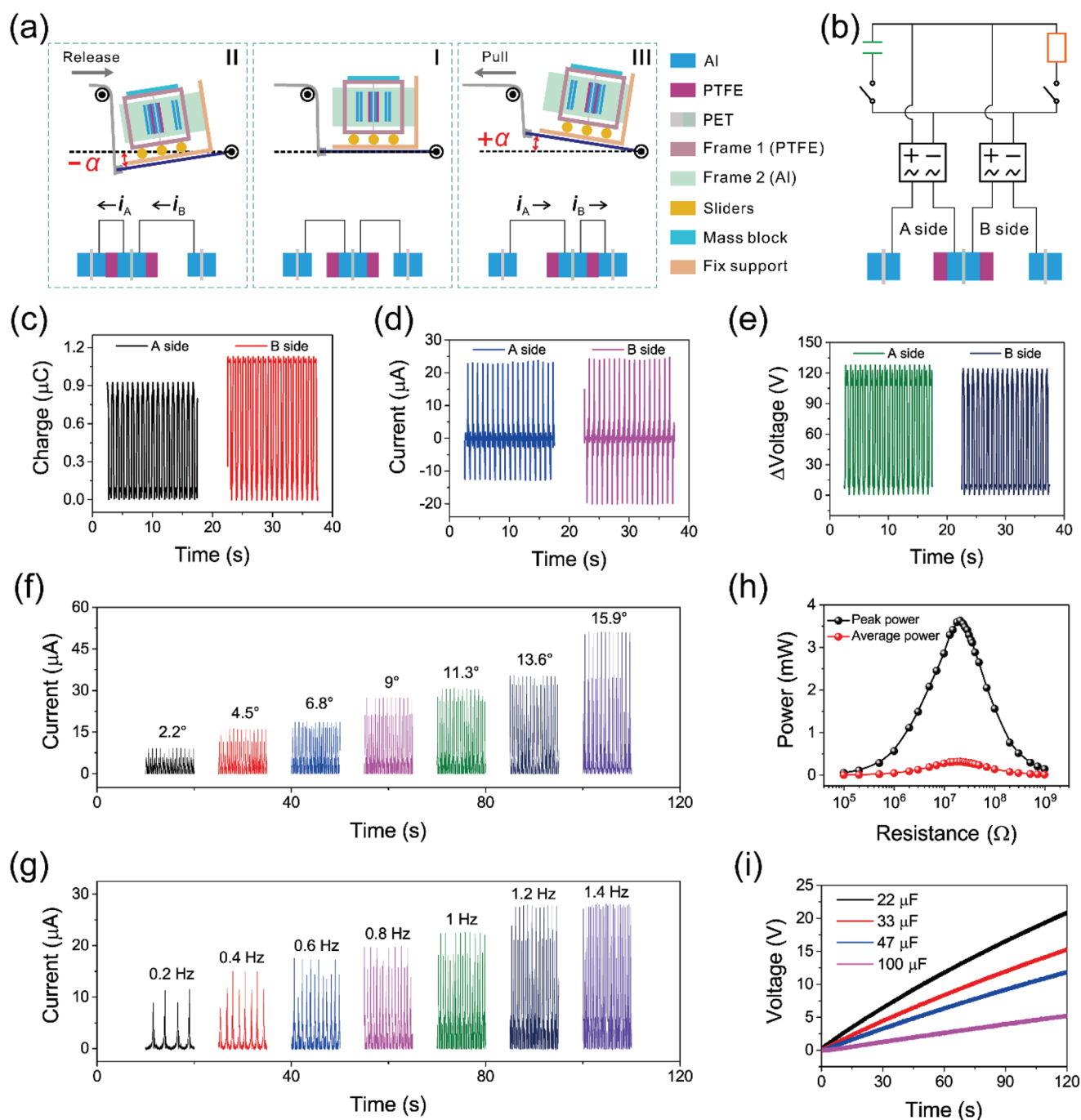


**Figure 2.** Basic characterization of the TS-TENG in air. a) Schematic illustration of the experimental setup. b) Rectification circuit diagram of the TS-TENG connected to different loads. Transferred charges c), short-circuit current d), and output voltage e) of the A side and B side, respectively. f) Rectified short-circuit current with different slopes. g) Rectified short-circuit current with different agitation frequencies. h) Peak power and average power of the TS-TENG. i) Charging performance of the TS-TENG to different capacitors. The agitation frequency is 1.2 Hz and the slope is 9° unless otherwise specified.

is also at rest. When the ship tilts to the left, the action point of the gravity remains the same, and the action point of the buoyancy moves to the right, also providing a torque to restore the ship (State III). In such a case, Frame 1 in the TS-TENG will slide to the right. In the experiments, a model ship was used with the TS-TENG mounted on the center of the bottom area. First, the response of the device under an initial tilt and succeeding free vibrations of the model ship in water

of the buoyancy moves to the right, also providing a torque to restore the ship (State III). In such a case, Frame 1 in the TS-TENG will slide to the right. In the experiments, a model ship was used with the TS-TENG mounted on the center of the bottom area. First, the response of the device under an initial tilt and succeeding free vibrations of the model ship in water

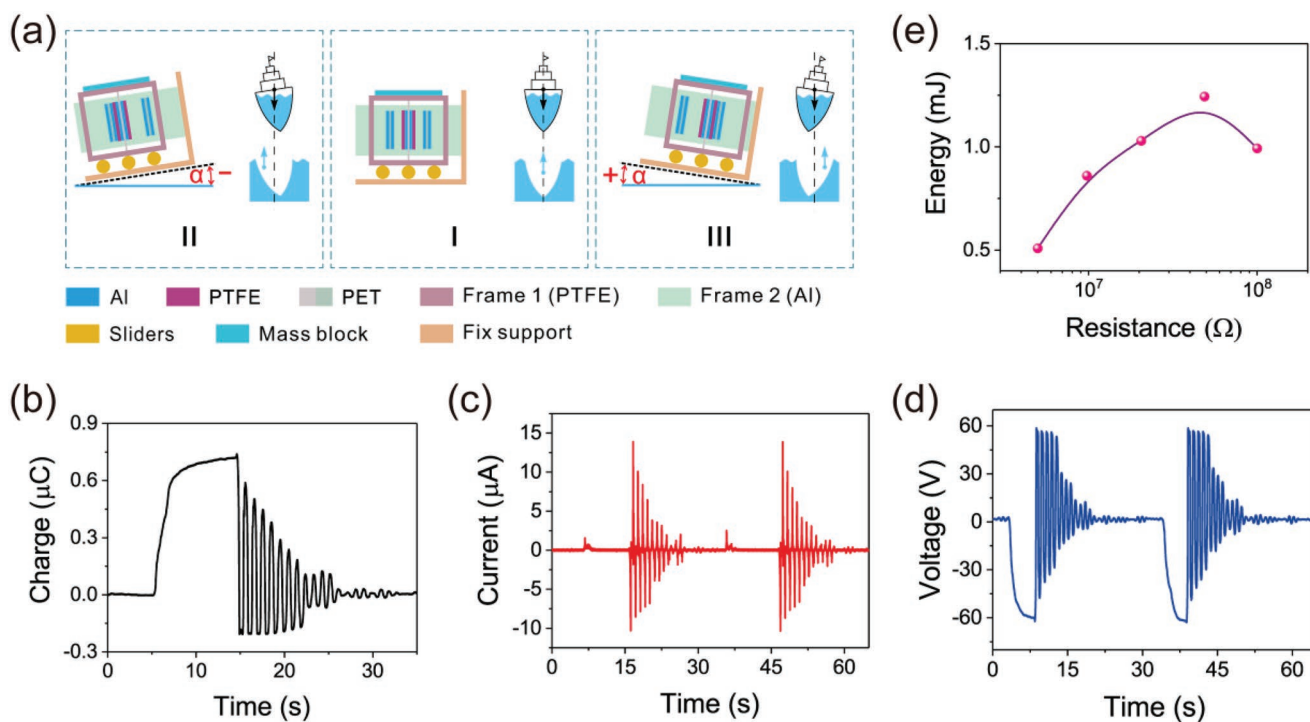


**Figure 3.** Output of the shipborne device with free vibration in water. a) Schematic illustration of the ship sway. Transferred charges b), short-circuit current c), and output voltage d) of the A side of the TS-TENG on a model ship with free vibration. e) Total output energy of the TS-TENG with three angular offset agitations. The offset angle is  $8.6^\circ$ .

was tested. The model ship was first tilted at an angle of  $8.6^\circ$  and then released, causing the ship to sway multiple times before stop. The output of the A side of the TS-TENG was characterized, as shown in Figure 3b–d. The transferred charges of the TS-TENG are  $0.8 \mu\text{C}$  initially, which decline and disappear after 11 obvious oscillations (Figure 3b). The short-circuit current is  $13.89 \mu\text{A}$  and disappears after 11 obvious oscillations (Figure 3c). The peak-to-peak voltage is  $105.25 \text{ V}$  initially (Figure 3d). The generated output signals have a good repeatability among two tilt agitations (Figure 3c,d), indicating that the TS-TENG can be also applied as a tilt sensor of the ship besides as an energy harvester. The total output energy of the TS-TENG under tilt agitations with different resistive loads is shown in Figure 3e. During three agitations by tilting the model ship to about  $8.6^\circ$ , the maximum output electrical energy of the whole device including the A and B sides is  $1.24 \text{ mJ}$  with a resistive load of  $48.8 \text{ M}\Omega$ . And the energy is calculated according to the following equation

$$E = \int_0^{T_E} I^2 R dt \quad (3)$$

where  $T_E$  is the output time span considered.

The response of the shipborne TS-TENG agitated by water waves was further studied. A wave tank was used to stimulate the tilts of the ship with nine wave makers. The amplitude of the water wave is tuned by the voltage of the control signal of the wave maker. The higher the voltage is, the larger the amplitude of the water wave becomes. Schematics of the ship sway in water waves and corresponding statuses of the

shipborne device are shown in Figure 4a. Such ship tilts have a large amount of mechanical energy that can be harvested and applied in practice. The rectified current of the shipborne device was studied in details with low wave frequencies of  $0.4\text{--}1.4 \text{ Hz}$  and low agitation amplitudes of  $1.5\text{--}2.5 \text{ V}$ . When the agitation amplitude was fixed at  $2.5 \text{ V}$ , the rectified current showed an approximate trend of gradually increasing with frequencies until the maximum value occurred at  $1.2 \text{ Hz}$  where the ship had violent sway, reaching  $25.04 \mu\text{A}$  (Figure 4b). When the frequency was fixed at  $1.2 \text{ Hz}$ , the rectified current gradually increased with amplitudes, and the maximum value is  $24.62 \mu\text{A}$  at the agitation amplitude of  $2.5 \text{ V}$  (Figure 4c). The response of the device to wide frequencies and amplitudes indicates its ability to sustain power generation in a variety of wave environments. The transferred charges of the whole TS-TENG are  $2.2 \mu\text{C}$  (half-cycle) at the frequency of  $1.2 \text{ Hz}$  and the agitation amplitude of  $2.5 \text{ V}$  (Figure 4d). The output voltage is  $301 \text{ V}$  with a resistive load of  $0.98 \text{ G}\Omega$  (Figure 4e). The peak power and average power of the whole shipborne device are  $1.8$  and  $0.23 \text{ mW}$  with optimal resistive loads of  $16.8$  and  $20.6 \text{ M}\Omega$ , respectively (Figure 4f).

Symmetrical structure is useful for achieving better motion stability and device scalability. Structural symmetry method based on rotational symmetry is first proposed to multiply the output and optimize the structure. As shown in Figure 5a, because the gravity of the slidable portion of the TS-TENG is mainly concentrated on the mass block, a complementary inverted device through rotational symmetry can improve motion stability of the combined two devices (Schematic I) by excluding extra torque on the sliders. Figure 5b shows a

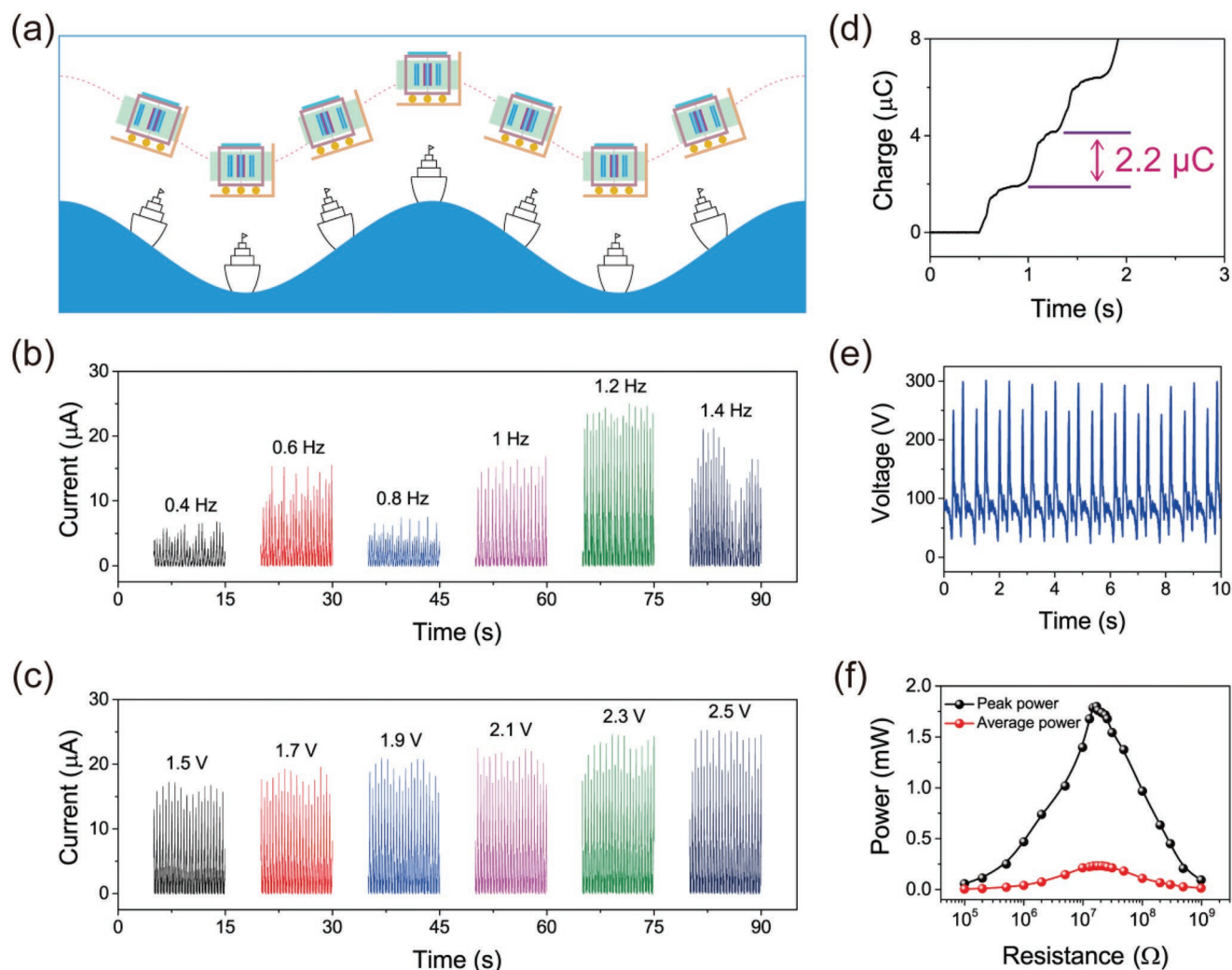


**Figure 4.** Output performance of the shipborne device in water. a) Schematic illustration of the working principle of the device on a ship. b) Rectified short-circuit current of the whole device with different wave frequencies. c) Rectified short-circuit current of the whole device with different wave amplitudes. d) Transferred charges of the whole device with the rectification circuit. e) Output voltage of the whole device with the rectification circuit. f) Peak power and average power of the TS-TENG. The agitation frequency is 1.2 Hz and the input voltage amplitude is 2.5 V unless otherwise specified.

fabricated inverted device. The output of the inverted device was also characterized at the wave frequency of 1.2 Hz and the agitation amplitude of 2.5 V. The rectified transferred charges (half-cycle) of the inverted device in water is 2.3  $\mu\text{C}$  (Figure 5c). The peak rectified current is 25.97  $\mu\text{A}$  (Figure 5d), and the output voltage is 302.87 V (Figure 5e). The peak power and average power are 2.84 and 0.2 mW, respectively, and the optimal matching resistance is about 20.6 M $\Omega$ . Taking the device volume into account, the peak power density and average power density are 1.41 and 0.1  $\text{W m}^{-3}$ , respectively. The basic outputs show that the inverted device can also have good performance. To demonstrate the electricity generation more intuitively, the inverted device was adopted to drive 30 LEDs successfully, as shown in Figure 5g and Video S1 (Supporting Information). For driving electronic devices requiring high power supply, the charging performance of the TS-TENG to different capacitors was tested in water wave environment.

A capacitor of 100  $\mu\text{F}$  can be charged to 3.74 V for only 120 s. The device can be integrated in a large scale, which is able to multiply the output for various applications on the ship, such as self-powered sensing for smart ships. Besides catching the sway energy of the ship, the TS-TENG is also possible to harvest wave energy directly, even to be applied in a power generation ship that only loads TS-TENGs to catch water wave energy. Moreover, the excellent ability of the TS-TENG to sense tilts can be used in a wide range of tilting sensing applications, such as earthquake warning, land sliding warning and bridge structure monitoring, etc.

### 3. Conclusions

In this work, a tilting-sensitive triboelectric nanogenerator is demonstrated for harvesting energy from unstable/fluctuating

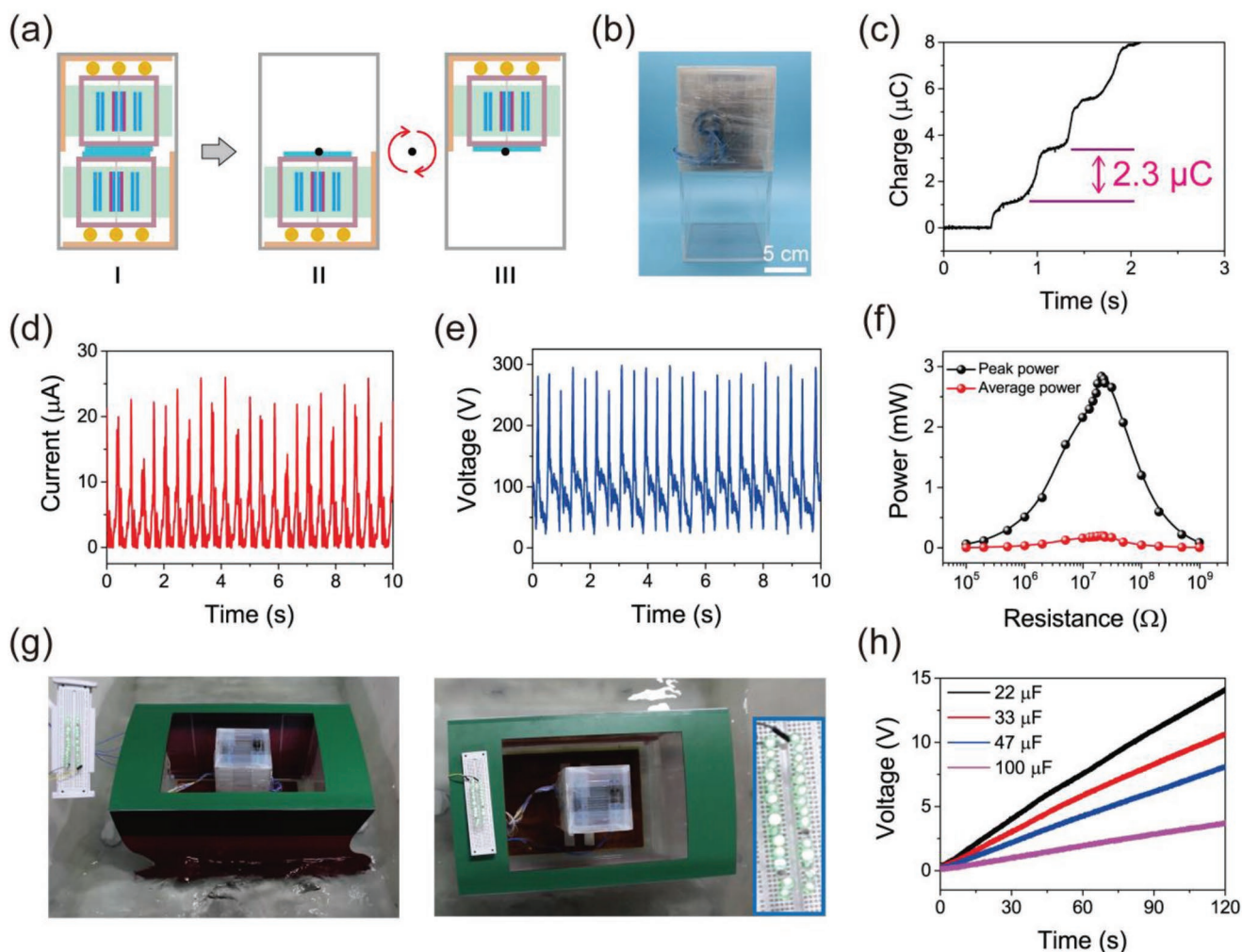


**Figure 5.** Output performance of the complementary inverted shipborne device in water. a) Schematic diagram of the complementary inverted device. b) Photograph of the complementary device. Transferred charges c), short-circuit current d), and output voltage e) of the whole device with rectification. f) Peak power and average power of the TS-TENG. g) Photographs of the device on a model ship powering LEDs in water. h) Charging performance of the TS-TENG to different capacitors. The agitation frequency is 1.2 Hz and the input voltage amplitude is 2.5 V.

surfaces, making use of the sway energy of ships. The device adopts integrated blade structures on sliders, which make it sensitive to tilts and guarantee its power output. The response of the device to tilt agitations of different slopes and frequencies are systematically investigated. Model ship experiments in wave tanks provide its output characteristics in water. The performance of the device demonstrates its high sensitivity to tilting. A complementary inverted device through rotational symmetry configuration is used to improve the motion stability of the device by excluding extra torque on the sliders. The peak power density and average power density of the TS-TENG can achieve 1.41 and 0.1  $\text{W m}^{-3}$ , respectively, in low-frequency and low-amplitude fluctuating conditions. By harvesting the sway energy of the ship, the device is promising for various applications on the ship, such as self-powered systems for smart ships. The excellent sensitivity of the TS-TENG to tilts can be applied in a wide range of slope sensing applications and energy harvesting from various unstable/fluctuating surfaces.

#### 4. Experimental Section

**Fabrication of the TS-TENG:** First, PET sheets (0.3 mm in thickness) were cut into the corresponding shape with a dimension of 116 mm  $\times$  80 mm. Al foils (82 mm  $\times$  80 mm, 50  $\mu\text{m}$  in thickness) were attached to the two sides of each PET sheet by pressure sensitive adhesive, forming the Al blade. Meanwhile, PTFE films (80  $\mu\text{m}$  in thickness) were adhered on the two sides of the Al blade, forming the PTFE blade. The PTFE films were corona charged by 3 kV for 5 min. There were 15 pieces of Al blades having an equal distance of 4.57 mm and 14 pieces of PTFE blades having an equal distance of 4.41 mm used in one TS-TENG. Frame 1 is a four-sided cuboid with a dimension of 88 mm  $\times$  88 mm  $\times$  106 mm, which was made of acrylic plates with thickness of 5 and 3 mm. Both ends of the PTFE blades were inserted into the top and bottom acrylic plates (5 mm) of the cuboid and fixed by folding. Frame 2 is also a four-sided cuboid with a dimension of 106 mm  $\times$  106 mm  $\times$  88 mm made of acrylic plates (5 and 3 mm in thickness). Both ends of the Al blades were inserted into the left and right acrylic plates (5 mm) of the cuboid and fixed by folding. The fix support is a cuboid that has three interconnected faces, and its dimension is 113 mm  $\times$  113 mm  $\times$  127 mm. Frame 2 was fixed on the side plates of the fix support. Two sliders were mounted on

the bottom plate of the fix support, and Frame 1 was fixed on the sliders. A metal block with a dimension of 95 mm × 104 mm × 8 mm and a mass of 695.4 g was fixed on the top of Frame 1. The above structures were assembled and packaged by a five-sided acrylic box with a dimension of 123 mm × 123 mm × 133 mm. The inner surface of the acrylic box was coated with a layer of water-proof glue, sealing the gaps in the walls of the box. The water-proof glue was applied by mixing two components with a ratio of 5:1. The wires of the TS-TENG were led out through holes in the acrylic box, which were also sealed with the water-proof glue. The rotationally symmetrical device used two such acrylic boxes, and the junction of the two boxes was fixed and sealed with PTFE tape.

**Fabrication of the Model Ship:** The main body of the model ship is a polypropylene box with a rectangular shape of 415 mm × 300 mm at the top and 400 mm × 290 mm at the bottom. The height of the box is 265 mm and the thickness of the wall is 2.06 mm. A rectangular copper plate with a dimension of 350.8 mm × 250.7 mm × 7.64 mm was placed at the bottom of the box to tune the mass of the ship. The side walls of the box were warped by ship-shaped plates.

**Device Characterization:** The output charges and the current of the TS-TENG and the voltage of capacitors were measured by an electrometer (Keithley 6514). The open-circuit voltage of the TS-TENG tested in air was also measured by the electrometer (Keithley 6514). The output voltage of the TS-TENG on the model ship was calculated by measuring the current through a resistive load of 0.98 GΩ using the electrometer (Keithley 6514). A linear motor (LinMot E1100) was used to agitate the TS-TENG in air. A function generator (Tektronix AFG3011C) was adopted to control the wave makers.

## Supporting Information

Supporting Information is available from the Wiley Online Library or from the author.

## Acknowledgements

W.Z. and L.X. contributed equally to this work. The research was supported by the National Key R & D Project from Minister of Science and Technology, China (2016YFA0202704), National Natural Science Foundation of China (Grant Nos. 51605033, 51735001, 51432005, 5151101243, and 51561145021), China Postdoctoral Science Foundation (Grant No. 2015M581041), and Beijing Municipal Science and Technology Commission (Grant Nos. Z171100002017017 and Y3993113DF).

## Conflict of Interest

The authors declare no conflict of interest.

## Keywords

energy harvesting, fluctuating surface, ship, sway energy, triboelectric nanogenerator

Received: July 2, 2019  
Revised: August 12, 2019  
Published online:

- [1] a) D. Gielen, F. Boshell, D. Saygin, *Nat. Mater.* **2016**, *15*, 117; b) Q. Schiermeier, J. Tollefson, T. Scully, A. Witze, O. Morton, *Nature* **2008**, *454*, 816.
- [2] a) Y. Zi, H. Guo, Z. Wen, M. H. Yeh, C. Hu, Z. L. Wang, *ACS Nano* **2016**, *10*, 4797; b) Z. L. Wang, *Mater. Today* **2017**, *20*, 74; c) J. Zhao, G. Zhen, G. Liu, T. Bu, W. Liu, X. Fu, P. Zhang, C. Zhang, Z. L. Wang, *Nano Energy* **2019**, *61*, 111.
- [3] a) F. R. Fan, Z. Q. Tian, Z. L. Wang, *Nano Energy* **2012**, *1*, 328; b) L. Xu, T. Z. Bu, X. D. Yang, C. Zhang, Z. L. Wang, *Nano Energy* **2018**, *49*, 625.
- [4] a) S. M. Niu, Z. L. Wang, *Nano Energy* **2015**, *14*, 161; b) Z. L. Wang, J. Chen, L. Lin, *Energy Environ. Sci.* **2015**, *8*, 2250.
- [5] a) L. Xu, T. Jiang, P. Lin, J. J. Shao, C. He, W. Zhong, X. Y. Chen, Z. L. Wang, *ACS Nano* **2018**, *12*, 1849; b) Z. L. Wang, *Nature* **2017**, *542*, 159; c) Z. L. Wang, T. Jiang, L. Xu, *Nano Energy* **2017**, *39*, 9; d) X. J. Zhao, S. Y. Kuang, Z. L. Wang, G. Zhu, *ACS Nano* **2018**, *12*, 4280.
- [6] a) B. Chen, Y. Yang, Z. L. Wang, *Adv. Energy Mater.* **2018**, *8*, 1702649; b) J. Bae, J. Lee, S. Kim, J. Ha, B. S. Lee, Y. Park, C. Choong, J. B. Kim, Z. L. Wang, H. Y. Kim, J. J. Park, U. I. Chung, *Nat. Commun.* **2014**, *5*, 4929.
- [7] a) J. Chen, Z. L. Wang, *Joule* **2017**, *1*, 480; b) X. F. Wang, S. M. Niu, F. Yi, Y. J. Yin, C. L. Hao, K. Dai, Y. Zhang, Z. You, Z. L. Wang, *ACS Nano* **2017**, *11*, 1728; c) M. Y. Xu, P. H. Wang, Y. C. Wang, S. L. Zhang, A. C. Wang, C. L. Zhang, Z. J. Wang, X. X. Pan, Z. L. Wang, *Adv. Energy Mater.* **2018**, *8*, 1702432.
- [8] a) B. D. Chen, W. Tang, T. Jiang, L. P. Zhu, X. Y. Chen, C. He, L. Xu, H. Y. Guo, P. Lin, D. Li, J. J. Shao, Z. L. Wang, *Nano Energy* **2018**, *45*, 380; b) J. Wang, S. M. Li, F. Yi, Y. L. Zi, J. Lin, X. F. Wang, Y. L. Xu, Z. L. Wang, *Nat. Commun.* **2016**, *7*, 12744; c) S. M. Niu, X. F. Wang, F. Yi, Y. S. Zhou, Z. L. Wang, *Nat. Commun.* **2015**, *6*, 8975.
- [9] a) L. Xu, H. Wu, G. Yao, L. B. Chen, X. D. Yang, B. D. Chen, X. Huang, W. Zhong, X. Y. Chen, Z. P. Yin, Z. L. Wang, *ACS Nano* **2018**, *12*, 10262; b) C. S. Wu, W. B. Ding, R. Y. Liu, J. Y. Wang, A. C. Wang, J. Wang, S. M. Li, Y. L. Zi, Z. L. Wang, *Mater. Today* **2018**, *21*, 216; c) X. Zhang, M. Yu, Z. Ma, H. Ouyang, Y. Zou, S. L. Zhang, H. Niu, X. Pan, M. Xu, Z. Li, Z. L. Wang, *Adv. Funct. Mater.* **2019**, *1900327*, <https://doi.org/10.1002/adfm.201900327>.
- [10] S. M. Niu, S. H. Wang, L. Lin, Y. Liu, Y. S. Zhou, Y. F. Hu, Z. L. Wang, *Energy Environ. Sci.* **2013**, *6*, 3576.
- [11] C. Zhang, W. Tang, C. B. Han, F. R. Fan, Z. L. Wang, *Adv. Mater.* **2014**, *26*, 3580.